EM fields generated by finite-length wire sources in 1D media: comparison with point dipole solutions

Rita Streich*† and Michael Becken*†,
*Potsdam University, Institute of Geosciences,
Karl-Liebknecht-Str. 24, 14476 Potsdam-Golm, Germany
†GFZ German Research Centre for Geosciences,
Telegrafenberg, 14473 Potsdam, Germany

ABSTRACT

In present-day land and marine controlled-source electromagnetic (CSEM) surveys, EM fields are commonly generated using wires that are hundreds of meters long. Nevertheless, simulations of CSEM data often approximate these sources as point dipoles. Although this is justified for sufficiently large source-receiver distances, many real surveys include frequencies and distances at which the dipole approximation is inaccurate. For 1D layered media, EM fields for point dipole sources can be computed using well-known quasi-analytical solutions, and fields for sources of finite lengths can be synthesized by superposing point dipole fields. However, the calculation of numerous point dipole fields is computationally expensive, requiring a large number of numerical integral evaluations. We combine a more efficient representation of finite-length sources in terms of components related to the wire and its end points with very general expressions for EM fields in 1D layered media. We thus obtain a formulation that requires fewer numerical integrations than the superposition of dipole fields and permits source and receiver placement at any depth within the layer stack. Complex source geometries, such as wires bent due to surface obstructions, can be simulated by segmenting the wire and computing the responses for each segment separately. We first describe our finite-length wire expressions, and then present examples of EM fields due to finite-length wires for typical land and marine survey geometries and discuss differences to point dipole fields.

INTRODUCTION

Controlled-source electromagnetic (CSEM) surveys are a useful exploration tool, applicable, e.g., for exploring hydrocarbon reservoirs, geothermal reservoirs, or for characterizing and potentially monitoring sites considered for carbon sequestration. A multitude of active electromagnetic sources are available, including magnetic loops (Frischknecht et al., 1991; Spies and Frischknecht, 1991) and long wires, grounded in land-based surveys (Strack, 1992; Wright et al., 2002; Ziolkowski et al., 2007) and deployed at the seafloor (Edwards, 2005) or towed through the water (e.g., Constable and Srnka, 2007) in marine surveys. Wire sources with lengths of several 100 m are most commonly used in commercial hydrocarbon exploration because of their capability to generate three-dimensional electrical current systems sensitive to both resistive and conductive, relatively deep targets (Spies and Frischknecht, 1991; Constable and Srnka, 2007).

In processing, inversion and interpretation of CSEM data, the sources are commonly approximated as point dipoles (e.g., Edwards, 1997; Johansen et al., 2005; Ziolkowski et al., 2007). This is adequate for sufficiently large source-receiver distances. However, real surveys targeting increasingly deep and small structures may include distances and frequencies at which the inaccuracy of the dipole approximation is on the order of (or larger than) the target-related anomalies. In such cases, it is vital to consider the actual source geometry.

For horizontally layered media, EM fields can be computed using well-known quasi-analytical solutions that involve numerical evaluations of Bessel function integrals (e.g., Weidelt, 2007; Løseth and Ursin, 2007). Using such point dipole solutions, EM fields due to finite-length wire sources can be synthesized by representing the wire as a line of point dipoles and summing the dipole fields. However, this procedure is computationally expensive, requiring many numerical integrations to calculate all of the point dipole contributions.

To improve the efficiency of long-wire source simulations, Soerensen and Christensen (1994) derived integrated Hankel integral expressions for finite-length wires that barely require more integral evaluations than the computation of point dipole fields. However, their approach includes elaborate computations of filter coefficients for every source-receiver pair. Another approach that reduces the number of integrations from that required for summing dipole fields is the separation of EM fields due to long wires into contributions from the wire and its end points (Ward and Hohmann, 1987). This technique works with standard Hankel filters. Whereas previous application of this approach considered subsurface receivers and sources located at the air-ground interface (Ward and Hohmann, 1987), we have applied it to a more general 1D field formulation that permits source and receiver positions at arbitrary depths within the layer stack (Løseth and Ursin, 2007). This allows simulations of finite marine sources in addition to land sources.

In this contribution, we first describe our finite-length wire representation. We then show examples of EM fields due to finite-length wires in representative land and marine settings over the frequency and distance ranges of typical CSEM surveys, and discuss differences to the fields due to infinitesimal dipoles.

EM FIELD EXPRESSIONS FOR FINITE-LENGTH WIRES

Expressions for the electromagnetic field due to a finite-length wire can be obtained by representing the wire as a line of infinitesimal dipoles and integrating the dipole expressions along the length of the wire. Using the nomenclature of Løseth and Ursin (2007), the EM fields for an x-directed point dipole embedded in a 1D layered medium can be expressed in

a form convenient for later integration as (see Appendix A)

$$E_x = \frac{Idx}{4\pi}\left(\int_0^\infty \frac{-\mu_0}{\sqrt{p_z^r p_z^s}}\mathcal{R}_{11}^A \kappa J_0(\kappa r)\mathrm{d}\kappa + \partial_x\left\{\frac{x^r - x^s}{r}\int_0^\infty\left[\frac{\mu_0}{\sqrt{p_z^r p_z^s}}\mathcal{R}_{11}^A - \sqrt{\frac{p_z^r p_z^s}{\tilde{\varepsilon}^r\tilde{\varepsilon}^s}}\mathcal{R}_{22}^A\right]J_1(\kappa r)\mathrm{d}\kappa\right\}\right), \quad (1a)$$

$$E_y = \frac{Idx}{4\pi}\partial_x\left\{\frac{y^r - y^s}{r}\int_0^\infty\left[\frac{\mu_0}{\sqrt{p_z^r p_z^s}}\mathcal{R}_{11}^A - \sqrt{\frac{p_z^r p_z^s}{\tilde{\varepsilon}^r\tilde{\varepsilon}^s}}\mathcal{R}_{22}^A\right]J_1(\kappa r)\mathrm{d}\kappa\right\}, \quad (1b)$$

$$E_z = \frac{jIdx}{4\pi\omega\tilde{\varepsilon}^r}\partial_x\left\{\int_0^\infty\sqrt{\frac{\tilde{\varepsilon}^r\tilde{\varepsilon}^s}{p_z^r p_z^s}}\mathcal{R}_{22}^D \kappa J_0(\kappa r)\mathrm{d}\kappa\right\}, \quad (1c)$$

$$H_x = \frac{Idx}{4\pi}\partial_x\left\{\frac{y^r - y^s}{r}\int_0^\infty\left[\sqrt{\frac{p_z^r}{p_z^s}}\mathcal{R}_{11}^D - \sqrt{\frac{\tilde{\varepsilon}^r p_z^s}{\tilde{\varepsilon}^s p_z^r}}\mathcal{R}_{22}^D\right]J_1(\kappa r)\mathrm{d}\kappa\right\}, \quad (1d)$$

$$H_y = \frac{Idx}{4\pi}\left(\int_0^\infty\sqrt{\frac{p_z^r}{p_z^s}}\mathcal{R}_{11}^D \kappa J_0(\kappa r)\mathrm{d}\kappa - \partial_x\left\{\frac{x^r - x^s}{r}\int_0^\infty\left[\sqrt{\frac{p_z^r}{p_z^s}}\mathcal{R}_{11}^D - \sqrt{\frac{\tilde{\varepsilon}^r p_z^s}{\tilde{\varepsilon}^s p_z^r}}\mathcal{R}_{22}^D\right]J_1(\kappa r)\mathrm{d}\kappa\right\}\right), \quad (1e)$$

$$H_z = \frac{jIdx}{4\pi\omega\mu_0}\frac{y^r - y^s}{r}\int_0^\infty\frac{\mu_0}{\sqrt{p_z^r p_z^s}}\mathcal{R}_{11}^A \kappa^2 J_1(\kappa r)\mathrm{d}\kappa, \quad (1f)$$

where I is the source current, dx is the length of the source dipole, κ is the horizontal wavenumber, ω is the angular frequency, μ_0 is the vacuum magnetic permeability, $\tilde{\varepsilon}^{\{s,r\}} = \varepsilon^{\{s,r\}} + j\sigma^{\{s,r\}}/\omega$ are the dielectric permittivity and electric conductivity of the source and receiver layer, respectively, $p_z^{\{s,r\}} = \sqrt{\mu_0\tilde{\varepsilon}^{\{s,r\}} - \kappa^2/\omega^2}$ are frequency-normalized vertical wavenumbers, $r = \sqrt{(x^r - x^s)^2 + (y^r - y^s)^2}$ is the horizontal source-receiver distance, and J_0 and J_1 are the zero- and first-order Bessel functions. $\mathcal{R}_{11}^A$, $\mathcal{R}_{22}^A$, $\mathcal{R}_{11}^D$ and $\mathcal{R}_{22}^D$ are the reflection responses of the layered medium as given by Løseth and Ursin (2007, their Equation 134). These quantities are computed recursively using the properties and thicknesses of all layers and the source and receiver depths. Subscripts 11 denote the TE-mode and subscripts 22 the TM-mode responses. Slightly different expressions apply for receivers below (Equations 134a and b) and above the source (Equations 134c and d of Løseth and Ursin, 2007). In Equations (1), a spatial derivative ∂_x has been retained wherever possible.

To obtain electromagnetic fields for a finite-length wire, we integrate Equations (1) over the wire length. Assuming that the wire is parallel to the x-axis, we express the integrals as discrete sums over N wire elements of length Δx, located at (x_n, y^s, z^s). The derivatives ∂_x are replaced by $-\partial/\partial_{\Delta x}$ (Ward and Hohmann, 1987). Then the fields at receiver location

(x^r, y^r, z^r) are

$$
\begin{aligned}
E_x &= \frac{I}{4\pi}\sum_{n=1}^{N}\Delta x\int_0^\infty \frac{-\kappa\mu_0}{\sqrt{p_z^r p_z^s}}\mathcal{R}_{11}^A J_0(\kappa r_n)\,\mathrm{d}\kappa \\
&\quad -\frac{I}{4\pi}\sum_{m=1}^{2}(-1)^m\frac{x^r-x_m}{r_m}\int_0^\infty\left[\frac{\mu_0}{\sqrt{p_z^r p_z^s}}\mathcal{R}_{11}^A-\sqrt{\frac{p_z^r p_z^s}{\tilde{\varepsilon}^r\tilde{\varepsilon}^r}}\mathcal{R}_{22}^A\right]J_1(\kappa r_m)\,\mathrm{d}\kappa, \qquad (2a)\\
E_y &= -\frac{I}{4\pi}\sum_{m=1}^{2}(-1)^m\frac{y^r-y^s}{r_m}\int_0^\infty\left[\frac{\mu_0}{\sqrt{p_z^r p_z^s}}\mathcal{R}_{11}^A-\sqrt{\frac{p_z^r p_z^s}{\tilde{\varepsilon}^r\tilde{\varepsilon}^r}}\mathcal{R}_{22}^A\right]J_1(\kappa r_m)\,\mathrm{d}\kappa, \qquad (2b)\\
E_z &= -\frac{jI}{4\pi\omega\tilde{\varepsilon}^r}\sum_{m=1}^{2}(-1)^m\int_0^\infty\sqrt{\frac{\tilde{\varepsilon}^r p_z^s}{\tilde{\varepsilon}^s p_z^r}}\mathcal{R}_{22}^D\kappa J_0(\kappa r_m)\,\mathrm{d}\kappa, \qquad (2c)\\
H_x &= -\frac{I}{4\pi}\sum_{m=1}^{2}(-1)^m\frac{y^r-y^s}{r_m}\int_0^\infty\left[\sqrt{\frac{p_z^r}{p_z^s}}\mathcal{R}_{11}^D-\sqrt{\frac{\tilde{\varepsilon}^r p_z^s}{\tilde{\varepsilon}^s p_z^r}}\mathcal{R}_{22}^D\right]J_1(\kappa r_m)\,\mathrm{d}\kappa, \qquad (2d)\\
H_y &= \frac{I}{4\pi}\sum_{n=1}^{N}\Delta x\int_0^\infty\sqrt{\frac{p_z^r}{p_z^s}}\mathcal{R}_{11}^D\kappa J_0(\kappa r_n)\,\mathrm{d}\kappa \\
&\quad +\frac{I}{4\pi}\sum_{m=1}^{2}(-1)^m\frac{x^r-x_m}{r_m}\int_0^\infty\left[\sqrt{\frac{p_z^r}{p_z^s}}\mathcal{R}_{11}^D-\sqrt{\frac{\tilde{\varepsilon}^r p_z^s}{\tilde{\varepsilon}^s p_z^r}}\mathcal{R}_{22}^D\right]J_1(\kappa r_m)\,\mathrm{d}\kappa, \qquad (2e)\\
H_z &= \frac{jI(y^r-y^s)}{4\pi\mu_0\omega}\sum_{n=1}^{N}\frac{\Delta x}{r_n}\int_0^\infty\frac{\mu_0}{\sqrt{p_z^r p_z^s}}\mathcal{R}_{11}^A\kappa^2 J_1(\kappa r_n)\,\mathrm{d}\kappa. \qquad (2f)
\end{aligned}
$$

For E_x, H_y and H_z, we obtain a contribution from each wire element. This contribution is described by the first sum in Equations 2a, 2e and 2f, with the distance between the receiver and the n^{th} wire element given by $r_n = \sqrt{(x^r - x_n)^2 + (y^r - y^s)^2}$. Upon integrating those terms of Equations (1) that contain derivatives ∂_x, the derivatives disappear, and we obtain explicit contributions from the integration limits, i.e., the end points of the wire. In Equations (2), the end point contributions are given by the summation over m ($m \in \{1, 2\}$), with the distances between the receiver and the wire ends denoted r_m.

To compute all EM field components for a finite-length wire using Equation (2), we have to evaluate three different integrals over the entire wire length. Accordingly, for a wire discretized into N elements, the number of numerical integral evaluations is approximately $3N$. In contrast, Equation (A-7) shows that two different integrals are required for computing only E_x for an infinitesimal dipole. The computation of all electromagnetic field components for a horizontal electric point dipole source requires numerical evaluations of eight different integrals (Løseth and Ursin, 2007). This would result in $8N$ numerical integrations when calculating finite-length wire fields from the contributions of N dipole elements. Compared to the simple summation of dipole fields, the separate computation of wire and end point contributions thus reduces the computational effort by more than 60%.

EXAMPLES

We use the expressions of EM fields due to finite-length wires given in Equation (2) to assess differences between the fields of finite sources and point dipoles for different representative experimental settings of land and marine surveys.

Land survey: straight grounded wire

We have simulated a land survey using the setup depicted in Figure 1. The electric conductivity model is based on the situation at the CO_2 sequestration pilot site in Ketzin, Germany, using measured conductivity values and the actual depth and thickness of the layer into which CO_2 is being injected (Giese et al., 2009). To simulate a realistic survey, in which sensors would typically be buried just below the surface, we placed electric and magnetic field receivers at a depth of 0.15 m. EM fields were computed for an infinitesimal dipole source at $(x, y) = (0, 0)$ and a 1-km long finite-length wire centered at $(x, y) = (0, 0)$. Both sources were located at a depth of 0.1 m.

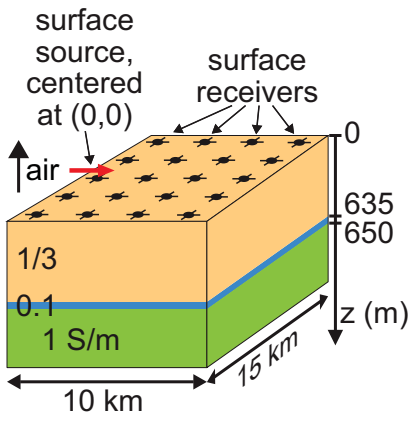

Figure 1: The 1D conductivity model and survey geometry used for simulating a land CSEM survey. The red arrow indicates the point dipole or 1000-m long wire source, centered at $(x, y) = (0, 0)$ and located 0.1 m below the surface. Receivers are located 0.15 m below the surface.

For convenience in the numerical simulations, we place the entire wire at a constant depth, either above or below the air-ground interface, although in real field surveys, grounded wires would typically be used, with the wire laid out on the surface and the end points coupled into the ground, e.g., via metal electrodes. The contribution from the wire body is typically smaller than that from the grounding points, and varies slowly as the wire depth crosses interfaces. Therefore, this simplification does not cause noticeable errors.

In Figure 2, we display the electric field component E_x at a frequency of 0.1 Hz for the model depicted in Figure 1. The finite-wire and point dipole fields differ significantly within a radius of $\sim$ 4 km from the source. Large relative differences also occur in the lowest-amplitude regions at oblique angles to the source; however, these are insignificant, because in these regions, E_x would not be measurable.

For comparison, we show in Figure 3 the electric field for the reservoir model of Fig-

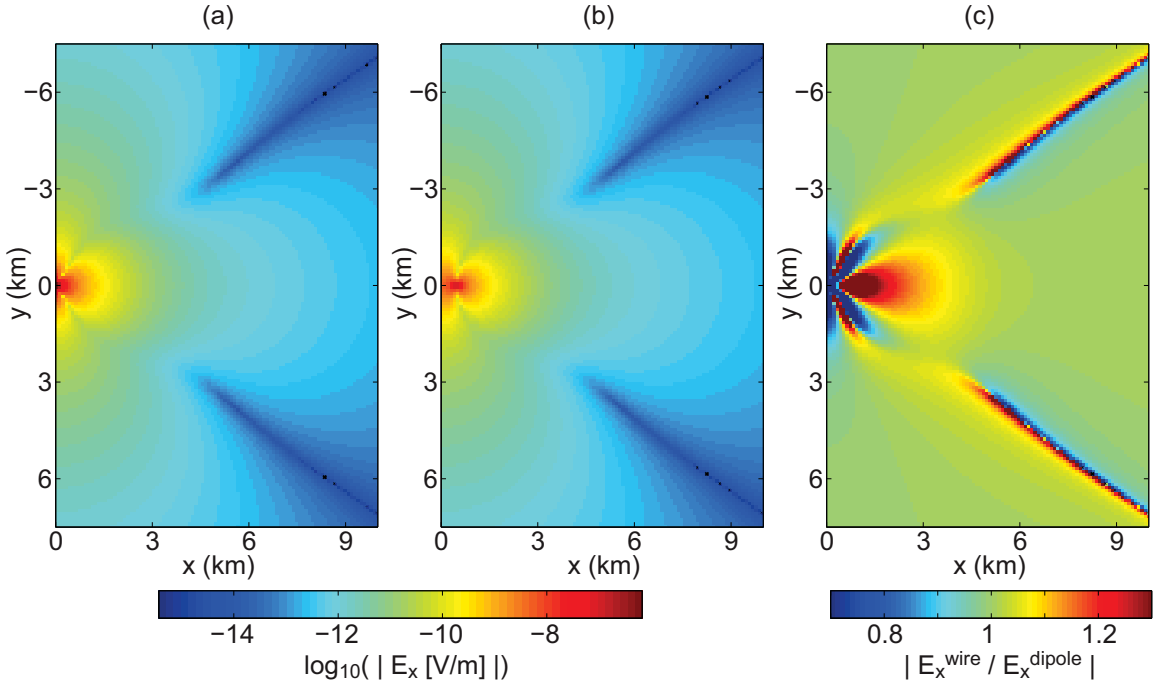

Figure 2: Electric field E_x for the configuration shown in Figure 1, a frequency of 0.1 Hz and (a) a point dipole source at $(0, 0, 0.1)$ m and (b) a 1000-m long grounded wire extending from $(-500, 0, 0.1)$ to $(500, 0, 0.1)$ m. (c) shows the ratio between the finite-length wire and point dipole fields.

ure 1 relative to the electric field for a model that does not contain a resistive layer. This demonstrates the size of the anomaly we would attempt to detect in the CSEM survey. The reservoir-related anomaly is smaller than the relative differences between finite-length wire and dipole fields, and overlaps spatially with the region in which the response is significantly influenced by the source geometry. This clearly indicates the importance of considering the true source geometry.

Similar observations can be made over a wide frequency range. In Figure 4, we compare the electric field E_x for finite-length and point dipole sources, and for the reservoir and background models, at frequencies of 0.001 Hz and 1 Hz. Significant differences between finite-length and point dipole sources occur in a similar region as for $f = 0.1$ Hz (compare Figures 4a and b to Figure 2c). The reservoir-related anomalies are somewhat smaller than for $f = 0.1$ Hz, underlining again that it is vital to consider the actual source length when searching for such relatively small anomalies.

In Figure 5, we display the finite-length wire fields for the E_y and E_z components, and their ratios to the respective point dipole fields. Here, the relative differences between the finite-length wire and point dipole fields are of similar size as for E_x. The regions in which the responses of finite-length wires and point dipoles differ significantly are similar, or slightly larger, in extent than for E_x. However, the amplitudes of E_z are considerably smaller than those of E_x and E_y, such that nearly the entire region in which E_z would be measurable (assuming instrument detection thresholds of $\sim 10^{-14} - 10^{-15}$, and possible measurement of E_z in shallow boreholes) is strongly influenced by the source geometry.

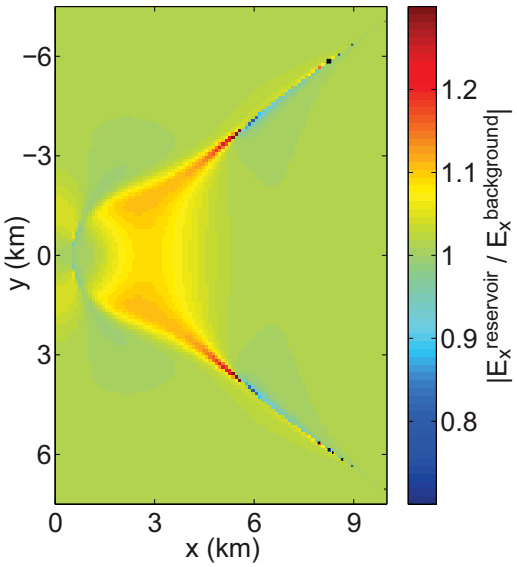

Figure 3: Electric field E_x for the configuration shown in Figure 1, a 1000-m long wire source and $f = 0.1$ Hz, normalized by the electric field for a background model not containing a resistive layer.

Required wire discretization

To minimize the computational effort, we have empirically investigated the effects of wire discretization on the resulting electromagnetic field values. In Figure 6, we display differences between a reference field E_x computed for a 1000-m long wire discretized using an element length of 0.1 m, and more coarsely discretized wires with element lengths varying between 1 m and 50 m. As expected, differences between the reference field and fields computed using coarser discretizations increase as the element length increases. Nevertheless, at the lower frequency of 0.1 Hz (Figure 6a), differences are small for all tested element lengths. As expected, differences are larger at $f = 100$ Hz, with maximum differences occurring in the vicinity of the end point of the wire at $x = 500$ m.

From this test, we conclude that for the lower frequency, a coarse discretization of $\sim 20-50$ m would be sufficient, whereas for the higher frequency, the wire should be discretized using elements no longer than $\sim 2-5$ m. These results may serve as rough guidelines for further simulation studies, but actual required discretizations are likely to depend on the total wire length and the resistivity model. To exclude any discretization-related error, all results presented here were computed using somewhat too careful discretizations with element lengths of 1 m.

Non-straight grounded wire

In real field surveys, surface obstacles may preclude laying out the source wire in a straight line. We have therefore studied differences between the EM fields for straight and non-straight wire sources. EM fields for non-straight wires are calculated by segmenting the wire into straight sections, and computing the responses for each segment separately using

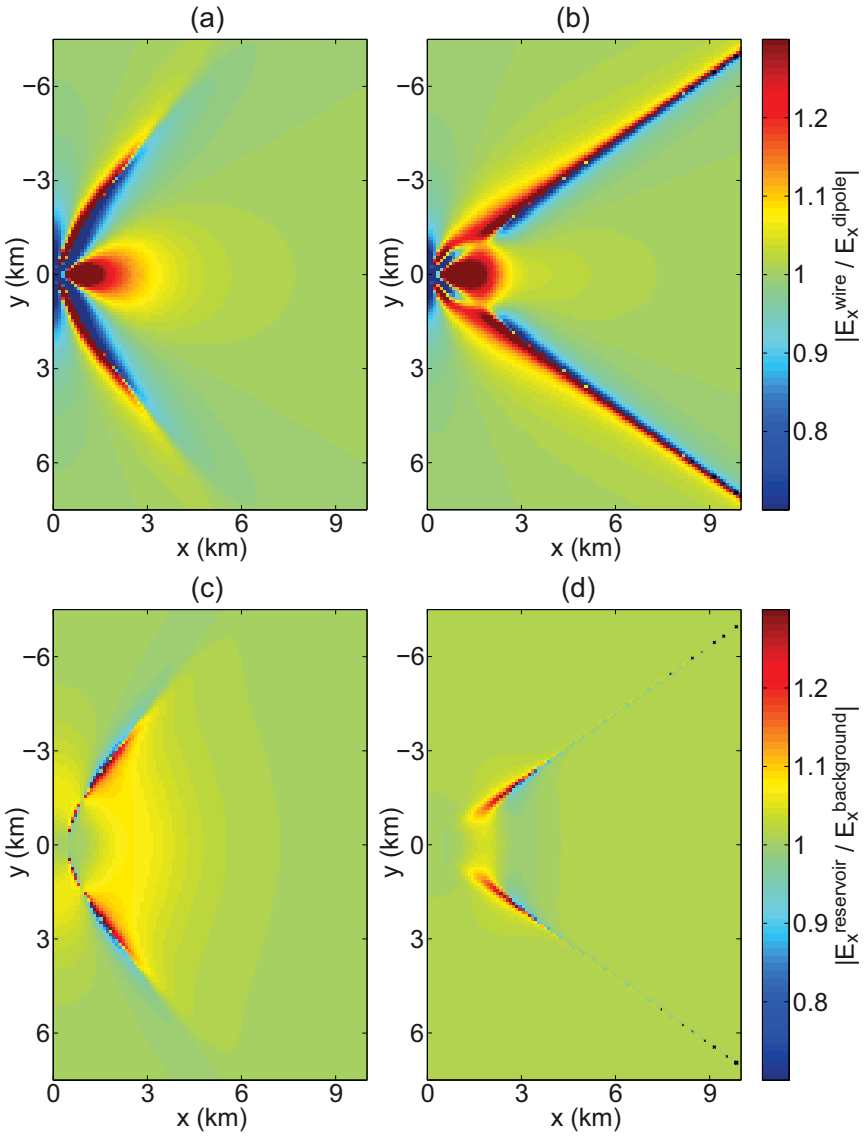

Figure 4: Ratio of E_x for a 1000-m long wire source to E_x for a point dipole for frequencies of (a) 0.001 Hz and (b) 1 Hz, and ratio of E_x for a 1000-m long wire source and the reservoir model shown in Figure 1 relative to E_x for a background model not containing the resistive layer for frequencies of (c) 0.001 Hz and (d) 1 Hz.

Equations (2) with appropriate rotations. As an example, we have computed the responses for a wire that consists of two segments arranged at a 120° angle. This wire has the same grounding points as the 1000-m long straight wire used previously. Figure 7 shows the wire geometry and the electric field E_x for the bent wire relative to E_x for a straight wire at frequencies of 0.001 Hz, 0.1 Hz and 1 Hz.

As expected, the E_x amplitudes for the bent wire are increased relative to the straight wire field at the side to which the wire is deviated ($y > 0$), and decreased at $y < 0$. Furthermore, relative differences between the bent and straight wire fields increase with increasing frequency, reaching a size similar to the reservoir-related anomaly for $f = 0.1$ Hz (com-

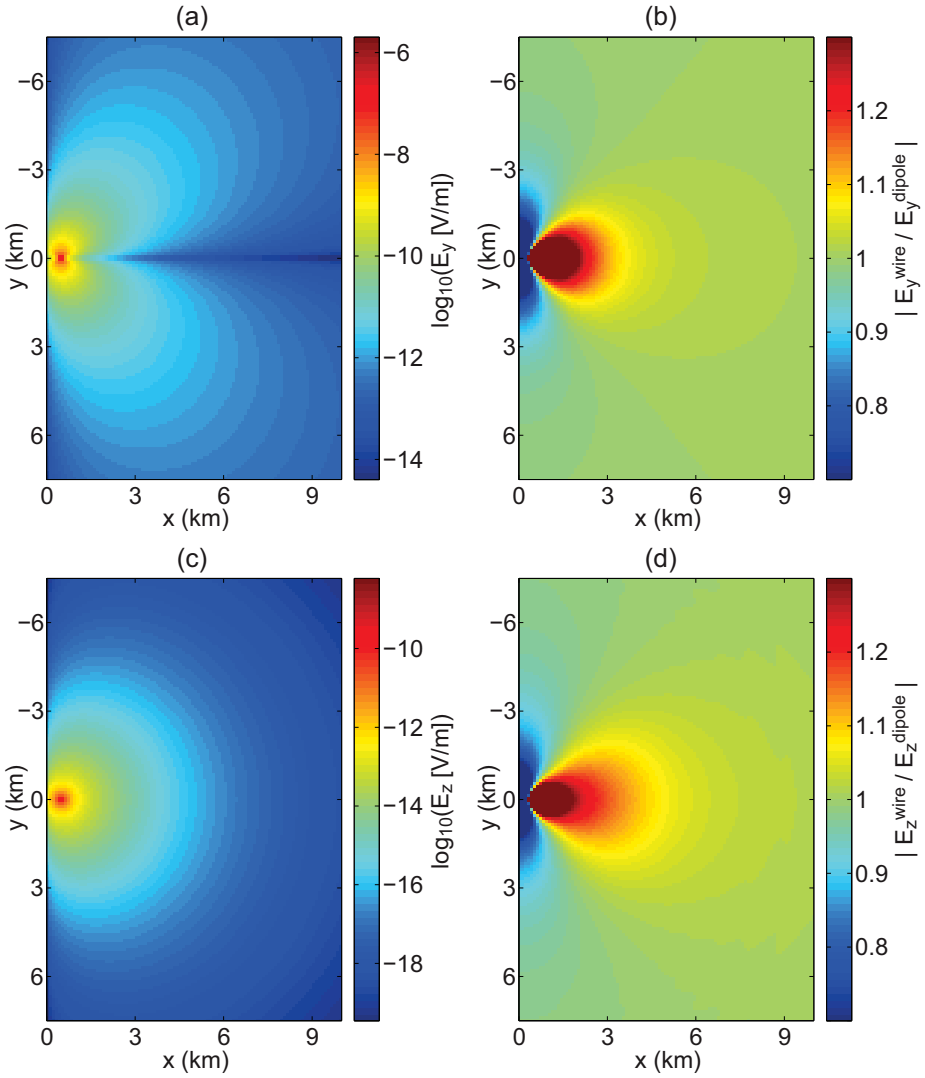

Figure 5: Electric field components (a) E_y and (c) E_z for the model shown in Figure 1 and a 1000-m long wire source at $f = 0.1$ Hz, and (b, d) the ratios of the finite-source E_y and E_z to the respective point dipole fields.

pare Figure 7b to 3), and larger than the reservoir-related anomaly for $f = 1$ Hz (compare Figure 7c to 4d). These results demonstrate that at these frequencies, the EM fields are significantly influenced not only by the grounding point locations, but also by the entire wire layout. In contrast, at $f = 0.001$ Hz, differences between bent and straight wire fields are barely visible (Figure 7a). At this low frequency, the electric field is similar to the potential field occurring in the DC limit (i.e., for $f = 0$). Here, the electric field is practically determined by the grounding point locations alone.

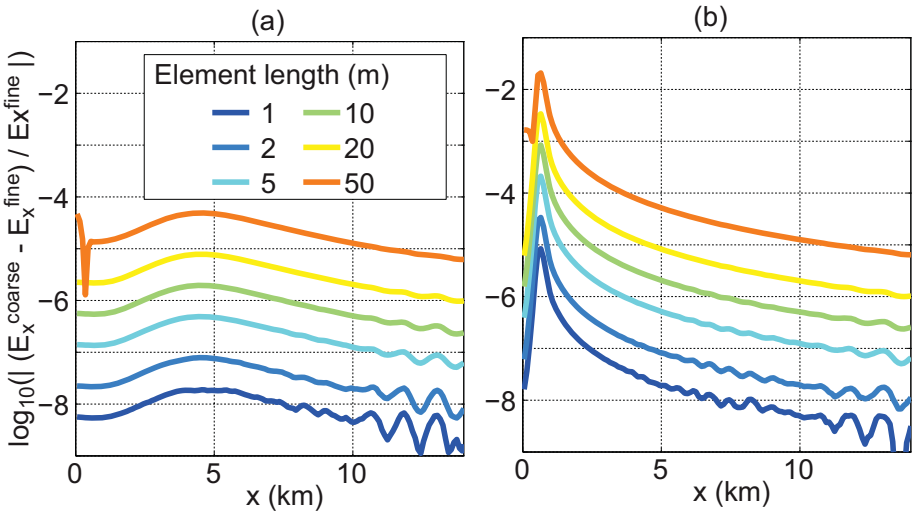

Figure 6: Relative differences between E_x^{coarse} computed for a 1000-m long wire using wire element lengths between 1 m and 50 m, and a reference field E_x^{fine} for a wire discretized using 0.1-m long elements, for frequencies of (a) 0.1 Hz and (b) 100 Hz. The resistivity model shown in Figure 1 was used, and field values were extracted along a line parallel to the source wire at a lateral offset of 50 m.

Marine survey: floating wire

Finite electric dipole sources used in marine CSEM surveys for commercial hydrocarbon exploration are typically $\sim 100 - 300$ m long (Constable and Srnka, 2007). Accordingly, differences between the EM fields due to such finite-length sources and point dipole fields are expected to be somewhat smaller than those observed for the 1-km long wire considered in the land survey examples.

We have computed marine EM responses for the model shown in Figure 8, which contains a 200-m water column and a stack of sedimentary layers, into which a 100-m thick resistive layer, representing a hydrocarbon reservoir, is embedded at a depth of 800–900 m below the seafloor. We simulated a point dipole source located at $(x, y) = (0, 0)$ and a 300-m long wire source, also centered at $(0, 0)$. Both sources were located 50 m above the seafloor, and receivers were placed 0.01 m above the seafloor.

Electric field E_x data for this configuration due to the finite-length wire and point dipole sources are shown in Figures 9a and b, and finite-source E_x data for the reservoir model relative to E_x for a model not containing the resistive layer are displayed in Figure 9c. The finite-length wire and point dipole fields are nearly identical at radii larger than ~ 1 km from the source center. The anomaly due to the resistive layer is several times larger than the relative differences between the finite-length wire and point dipole fields, and is largest at distances well beyond the region significantly influenced by the source geometry. Therefore, the point dipole approximation may be adequate in this case. However, taking into account the exact source geometry may again become important when searching for smaller anomalies caused, e.g., by thinner reservoirs or relatively small 3D structures.

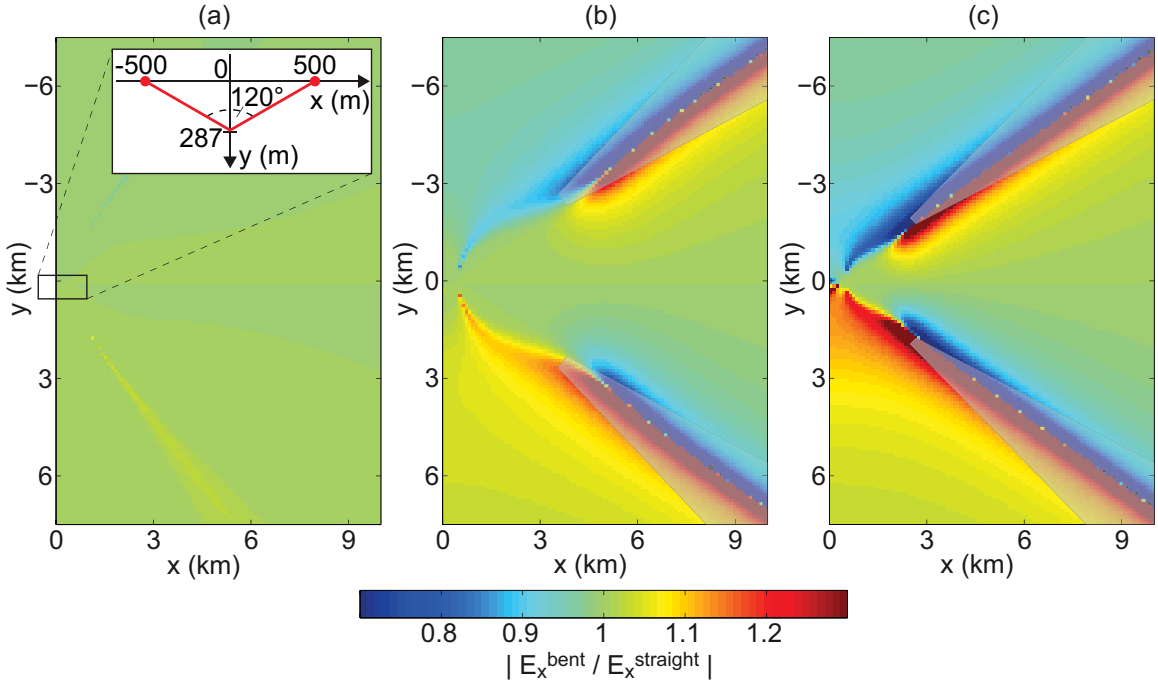

Figure 7: Electric field E_x for a bent wire. The inset in (a) shows the geometry of a wire that consists of two segments and has the same grounding points as the straight wire used previously. Shown is the ratio of E_x^{bent} for the bent wire to $E_x^{straight}$ for the straight wire at depth $z = 0.15$ m and frequencies of (a) 0.001 Hz, (b) 0.1 Hz and (c) 1 Hz. Gray shades in (b) and (c) roughly mark very low-amplitude regions in which E_x would not be measurable.

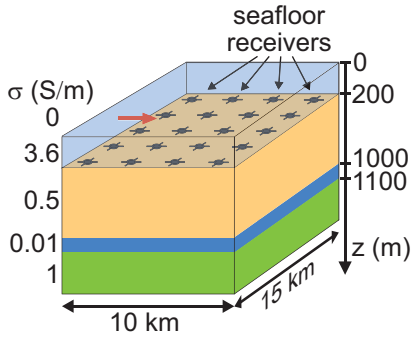

Figure 8: The 1D conductivity model and survey geometry used for simulating a marine CSEM survey. The red arrow indicates the point dipole or 300-m long wire source, centered at $(x, y) = (0, 0)$ and located 50 m above the seafloor. Receivers are located 0.01 m above the seafloor.

CONCLUSIONS

We have presented a formulation for computing electromagnetic fields due to electric dipole sources of finite extent by splitting the responses into contributions from the wire body and its end points. Being derived from a quite general representation of point dipole fields, our finite-length wire formulation allows us to compute EM fields in 1D layered media for

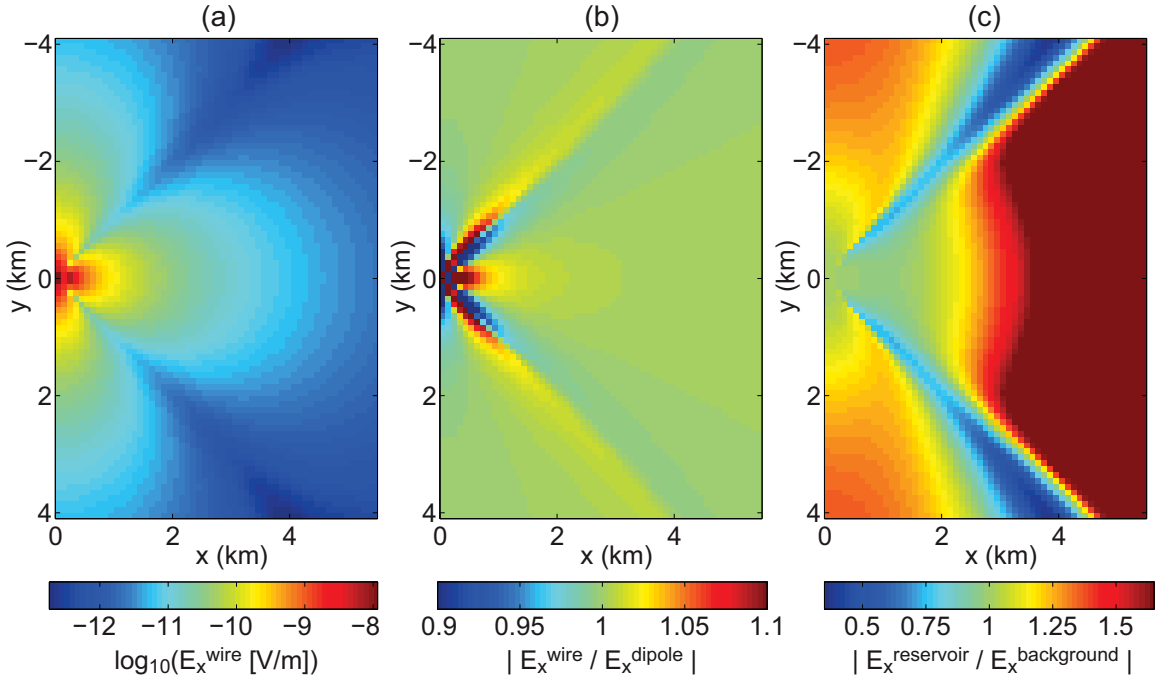

Figure 9: (a) Electric field E_x for a 300-m long wire source and the marine survey configuration shown in Figure 8 at $f = 0.1$ Hz. (b) The ratio between the finite-length wire field shown in (a) and the field due to a point dipole source. (c) The finite-length wire field for the reservoir model of Figure 8 relative to the background field for a model not containing the 100-m thick resistive layer. Note the different color scales in (b) and (c).

sources and receivers located at any depth. Compared to direct summation of dipole fields, we gain $\sim 60\%$ efficiency. Implementation is straightforward, as we only require integral evaluations via standard fast Hankel transforms, for which precomputed sets of coefficients are available.

The utility of the finite-length wire formulation has been demonstrated by presenting EM fields for several representative CSEM survey configurations. Our tests confirm that finite-length wire and point dipole fields can differ significantly over distance ranges reaching several times the wire length. For a simulated land CSEM survey targeting a thin resistive anomaly, comparison of the responses for a 1000-m long grounded wire source to point dipole responses shows that in this case, it is crucial to consider the actual source geometry. The anomalous response of the target structure is smaller than the relative differences between finite-length wire and point dipole fields, and overlaps spatially with the region in which the response is strongly influenced by the source geometry. Qualitatively similar deviations between finite-length wire and point dipole fields are observed over relatively wide frequency ranges and for different EM field components. At frequencies above the 'effective' DC limit, it is also important to consider the actual wire layout; knowledge of the grounding point positions is not sufficient for computing accurate responses.

In contrast, for the marine survey simulated, using a shorter wire and thicker target layer, the wire geometry only had a relatively small impact on the responses, and anomalies due to the target layer were spatially well separated from the region significantly influenced by

the source geometry. This indicates that the actual source geometry is of minor importance for the survey considered. Nevertheless, this cannot be generalized to other surveys aiming at detecting smaller target structures that generate weaker EM field anomalies.

Our 1D solution for finite-length wire sources can easily be incorporated into higher-dimensional CSEM modeling and inversion algorithms. Most 2D and 3D modeling schemes use a secondary field approach, in which primary fields for a simple (e.g., homogeneous or 1D) model are computed analytically, and secondary fields arising from deviations of the 2D or 3D resistivity model from the background model are computed numerically. Here, finite-length sources can be included into the background field computations.

ACKNOWLEDGMENTS

This work was funded by the German Federal Ministry of Education and Research within the framework of the GeoEn project.

APPENDIX A

EM FIELD EXPRESSIONS FOR POINT DIPOLES

We show the derivation of expressions for dipole EM fields in a form convenient for integration over the length of a source wire using the example of the E_x component. Analogous considerations apply for the other EM field components.

Using the nomenclature of Løseth and Ursin (2007), the space-frequency domain electric field E_x for an isotropic layered medium, with source and receiver embedded at arbitrary depth, is given by the double Fourier integral

$$E_x = -\frac{Idx}{8\pi^2}\int_{-\infty}^{\infty}\int_{-\infty}^{\infty}\left[\left(1-\frac{k_x^2}{\kappa^2}\right)\frac{\mu_0}{\sqrt{p_z^r p_z^s}}\mathcal{R}_{11}^A+\sqrt{\frac{p_z^r p_z^s}{\tilde{\varepsilon}^r\tilde{\varepsilon}^s}}\frac{k_x^2}{\kappa^2}\mathcal{R}_{22}^A\right]\exp\left\{j\left(k_x x+k_y y\right)\right\}\mathrm{d}k_x\mathrm{d}k_y, \quad \text{(A-1)}$$

where k_x and k_y are horizontal wavenumbers with $\kappa^2 = k_x^2 + k_y^2$, and the other symbols are the same as those explained for Equation (1).

Transformation to cylindrical coordinates using $k_x = \kappa\cos\alpha$, $k_y = \kappa\sin\alpha$, $x = r\cos\beta$, $y = r\sin\beta$, $\xi = \alpha - \beta + \pi/2$, $k_x^2 \to -\partial_x^2$, and substituting the zero-order Bessel function,

$$J_0\left(\kappa r\right) = \frac{1}{2\pi}\int_0^{2\pi} e^{j\kappa r\sin\xi}\mathrm{d}\xi, \quad \text{(A-2)}$$

results in

$$E_x = \frac{Idx}{4\pi}\left(\int_0^{\infty}\frac{-\mu_0}{\sqrt{p_z^r p_z^s}}\mathcal{R}_{11}^A\kappa J_0(\kappa r)\,\mathrm{d}\kappa-\partial_x^2\left\{\int_0^{\infty}\left[\frac{\mu_0}{\sqrt{p_z^r p_z^s}}\mathcal{R}_{11}^A-\sqrt{\frac{p_z^r p_z^s}{\tilde{\varepsilon}^r\tilde{\varepsilon}^s}}\mathcal{R}_{22}^A\right]\frac{1}{\kappa}J_0(\kappa r)\,\mathrm{d}\kappa\right\}\right). \quad \text{(A-3)}$$

After evaluating *one* of the spatial derivatives using (Ward and Hohmann, 1987)

$$\partial_x J_0\left(\kappa r\right) = -\frac{\kappa x}{r}J_1\left(\kappa r\right), \quad \text{(A-4)}$$

we obtain

$$E_x = \frac{Idx}{4\pi}\left(\int_0^\infty \frac{-\mu_0}{\sqrt{p_z^r p_z^s}}\mathcal{R}_{11}^A \kappa J_0(\kappa r)\,\mathrm{d}\kappa + \partial_x\left\{\frac{x}{r}\int_0^\infty\left[\frac{\mu_0}{\sqrt{p_z^r p_z^s}}\mathcal{R}_{11}^A - \sqrt{\frac{p_z^r p_z^s}{\tilde{\varepsilon}^r\tilde{\varepsilon}^s}}\mathcal{R}_{22}^A\right]\mathrm{d}\kappa\right\}\right). \quad \text{(A-5)}$$

Equation (A-5) is used as the basis for deriving the expressions for finite-length wire fields. Further evaluation of the second spatial derivative using

$$\partial_x J_1(\kappa r) = -\frac{x}{r^2}J_1(\kappa r) + \frac{\kappa x}{r}J_0(\kappa r) \quad \text{(A-6)}$$

results in an explicit expression for the point dipole field in terms of two different Hankel integrals:

$$\begin{aligned} E_x &= \frac{Idx}{4\pi}\left(\int_0^\infty\left[\left(\frac{x^2}{r^2}-1\right)\frac{\mu_0}{\sqrt{p_z^r p_z^s}}\mathcal{R}_{11}^A - \frac{x^2}{r^2}\sqrt{\frac{p_z^r p_z^s}{\tilde{\varepsilon}^r\tilde{\varepsilon}^r}}\mathcal{R}_{22}^A\right]\kappa J_0(\kappa r)\,\mathrm{d}\kappa\right. \\ &+ \left.\left(\frac{1}{r}-\frac{2x^2}{r^3}\right)\int_0^\infty\left[\frac{\mu_0}{\sqrt{p_z^r p_z^s}}\mathcal{R}_{11}^A - \sqrt{\frac{p_z^r p_z^s}{\tilde{\varepsilon}^r\tilde{\varepsilon}^r}}\mathcal{R}_{22}^A\right]J_1(\kappa r)\,\mathrm{d}\kappa\right). \quad \text{(A-7)} \end{aligned}$$

REFERENCES

Constable, S., and L. J. Srnka, 2007, An introduction to marine controlled-source electromagnetic methods for hydrocarbon exploration: Geophysics, **72**, WA3–WA12.

Edwards, N., 2005, Marine controlled source electromagnetics: Principles, methodologies, future commercial applications: Surveys in Geophysics, **26**, 675–700.

Edwards, R. N., 1997, On the resource evaluation of marine gas hydrate deposits using sea-floor transient electric dipole-dipole methods: Geophysics, **62**, 63–74.

Frischknecht, F. C., V. F. Labson, B. R. Spies, and W. L. Anderson, 1991, Profiling methods using small sources, *in* Electromagnetic Methods in Applied Geophysics: Society of Exploration Geophysicists, **2**, 105–270.

Giese, R., J. Henninges, S. Lüth, D. Morozova, C. Schmidt-Hattenberger, H. Würdemann, M. Zimmer, C. Cosma, C. Juhlin, and CO2SINK Group, 2009, Monitoring at the CO_2SINK site: A concept integrating geophysics, geochemistry and microbiology: Energy Procedia, **1**, 2251–2259.

Johansen, S. E., H. E. F. Amundsen, T. Røsten, S. Ellingsrud, T. Eidesmo, and A. H. Bhuyian, 2005, Subsurface hydrocarbons detected by electromagnetic sounding: First Break, **23**, 3136.

Løseth, L. O., and B. Ursin, 2007, Electromagnetic fields in planarly layered anisotropic media: Geophysical Journal International, **170**, 44–80.

Soerensen, K. I., and N. B. Christensen, 1994, The fields from a finite electrical dipole - A new computational approach: Geophysics, **59**, 864–880.

Spies, B. R., and F. C. Frischknecht, 1991, Electromagnetic sounding, *in* Electromagnetic Methods in Applied Geophysics: Society of Exploration Geophysicists, **2**, 285–425.

Strack, K. M., 1992, Exploration with deep transient electromagnetics: Elsevier.

Ward, S. H., and G. W. Hohmann, 1987, Electromagnetic theory for geophysical applications, *in* Electromagnetic Methods in Applied Geophysics: Society of Exploration Geophysicists, 131–311.

Weidelt, P., 2007, Guided waves in marine CSEM: Geophysical Journal International, **171**, 153–176.

Wright, D., A. Ziolkowski, and B. Hobbs, 2002, Hydrocarbon detection and monitoring with a multicomponent transient electromagnetic (MTEM) survey: The Leading Edge, **21**, 852–864.

Ziolkowski, A., B. A. Hobbs, and D. Wright, 2007, Multitransient electromagnetic demonstration survey in france: Geophysics, **72**, F197–F209.